ADVANCED ELECTRONIC MATERIALS Open Access
www.advelectronicmat.de

Toward All-Carbon Electronics Buried in Diamond

Calum S. Henderson, Patrick S. Salter, Emil T. Jonasson, and Richard B. Jackman*

This work investigates the use of femtosecond laser processing to fabricate various nanocarbon structures with distinct electrical behaviors within diamond substrates. Conventional approaches for achieving diamond doping have significant disadvantages, including challenging growth profiles, limited environmental stability, and sub-optimal psuedo-vertical structures. Here, it is demonstrated that laser-written nanocarbon networks (NCNs) directly alleviate these issues, demonstrating the highly repeatable fabrication of robust and precise electrical architectures buried in diamond with proven stability over repeated temperature and voltage cycling. By varying the laser pulse repetition rate (PRR), a transition from Ohmic conductive to semiconductive/ambipolar behavior is achieved in the modified diamond. Furthermore, a proof-of-concept, all-carbon transistor architecture buried within the bulk diamond is presented, showcasing the potential for integrated device fabrication using the laser-writing process.

1. Introduction

Ultra wide-bandgap (UWBG) semiconductors are increasingly recognized as critically important materials for future electronic device engineering. They promise vastly improved device performance due to their high breakdown voltages and potentially low ON-resistances, as evidenced by their superior figures of merit compared to conventional materials.[1,2] Among UWBG materials, such as gallium oxide and aluminum nitride, the remarkable properties of diamond make it stand out as the ideal material for extreme environment or high-power applications. Its resilience to environmental factors such as radiation or corrosives, coupled with its impressive electronic properties, are key to producing efficient, dependable, and long-lasting electronics.[3–5]

However, diamond's remarkable properties have historically been difficult to harness due to challenges in substrate synthesis and processing. Growth of commercially viable wafers, achieving reliable metal adhesion, and precise substrate patterning have been significant obstacles.[6] Recent advancements in plasma-enhanced chemical vapor deposition (CVD) techniques, doping control, substrate etching and interface management are gradually overcoming these challenges, bringing the widespread uptake of diamond electronics closer to reality.[7] Indeed, as each generation of diamond-based device improves upon the last, real-world applications have been identified. Diamond radiation detectors, for instance, are now operational in nuclear facilities worldwide.[8] Schottky diode structures with a current density, breakdown field, and rectification ratio of greater than 10^3 Acm^{-2}, 7.7 $MVcm^{-1}$, and 10^{12}, respectively, are now achievable, opening new avenues in power electronics.[9] Additionally, ever more complex and capable diamond transistors are being developed, utilizing both so-called surface transfer doping and conventional substitutional doping techniques.[10]

Substitutional doping, as is used in conventional silicon electronics can realize both n-type (nitrogen- or phosphorous-doped) and p-type (boron-doped) layers, and a range of devices have been successfully fabricated using this approach. However, these dopant atoms only offer very deep donor and acceptor states, giving activation energies of 1.7, 0.57, and 0.37 eV for nitrogen, phosphorous, and boron, respectively.[11–13] As a result, these devices are generally more suited to high-temperature operation, as current densities remain poor for room-temperature applications. Furthermore, due to ion migration during the high temperature diamond CVD process, the growth of discrete doped layers with sharp interfaces is challenging, further reducing the usefulness of this technology.

Hydrogen surface termination of the diamond crystal results in the formation of a p-type surface and is comparatively simple to achieve via hydrogen plasma treatment. Many research groups have reported hydrogen terminated devices with high

C. S. Henderson
London Centre for Nanotechnology
University College London (UCL)
17-19 Gordon Street, London WC1H 0AH, UK
E-mail: calum.henderson.19@ucl.ac.uk
P. S. Salter
Department of Engineering Science
University of Oxford
Oxford OX1 3PJ, UK
E. T. Jonasson
Remote Applications in Challenging Environments (RACE)
UK Atomic Energy Authority (UKAEA)
Culham Campus, Abingdon OX14 3DB, UK
R. B. Jackman
London Centre for Nanotechnology and the Department of Electronic and Electrical Engineering
University College London (UCL)
17-19 Gordon Street, London WC1H 0AH, UK
The ORCID identification number(s) for the author(s) of this article can be found under https://doi.org/10.1002/aelm.202500267

DOI: 10.1002/aelm.202500267

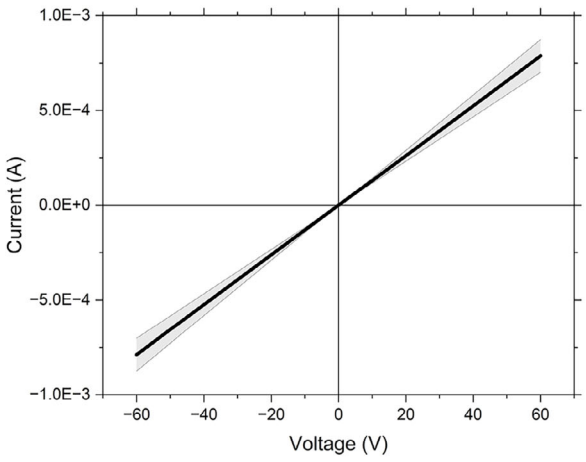

(a)

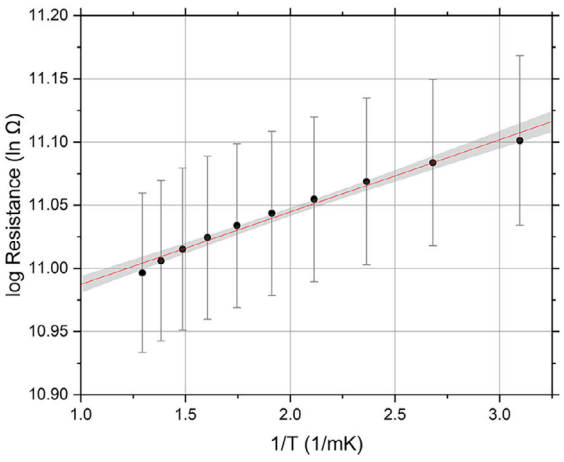

(b)

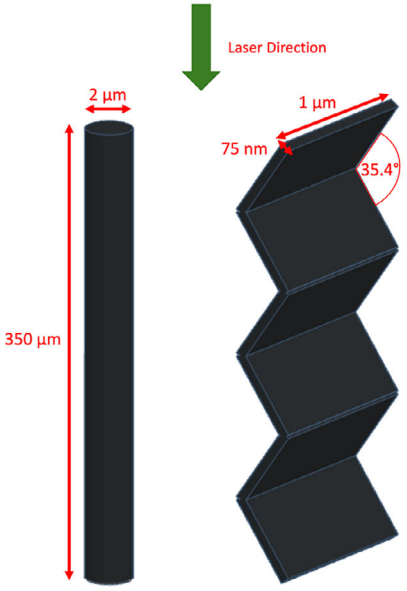

(c)

Figure 1. a) IV characteristics for the PRR-1k devices, showing a perfectly Ohmic voltage response with a resistance of 76(± 8) kΩ, and b) gives the Arrhenius plot for the PRR-1k device, providing an activation energy of 4.9(±0.2) meV. A single RC parallel circuit was used to fit the impedance spectra in order to find the system's resistance. The 95% confidence interval is shown as the shaded area. c) Alternative internal structure models for the conductive graphitic pathways within the NCN columns. The two primary models considered were (left) a solid graphitic cylinder akin to a traditional metallic conducting wire, and (right) a series of 75 nm thick sheets 35.4° off-axis, as has been observed in electron microscopy studies of laser-written material processed using the same parameters.

current densities, including FETs and Schottky diodes.[14,15] Previously, a significant drawback was that doping using a bare hydrogen terminated surface is somewhat transient, suffering from poor stability and a dependence on the local gaseous environment. This issue is addressed by the addition of a metal-oxide passivation layer over the hydrogen terminated surface, resulting in improved longevity and chemical & thermal stability.[16,17] In terms of the ultimate stability required for extreme environments and/or high-power applications, here an entirely new approach is proposed. This paper proposes the use of laser-fabricated, 3-D nanocarbon-network (NCN) structures embedded within the diamond substrate for use as the active regions of electronic devices.

By employing femtosecond laser-processing of diamond, electrically conductive architectures can be formed by the localized breakdown of the sp^3 material, without disrupting the surrounding crystal.[18,19] While the breakdown of the diamond lattice into other carbon allotropes can be driven by thermal effects using laser pulses longer than diamond's electron–phonon relaxation time (approx. 1 ps), this often leads to larger, less-confined cracks throughout the substrate, severely compromising the

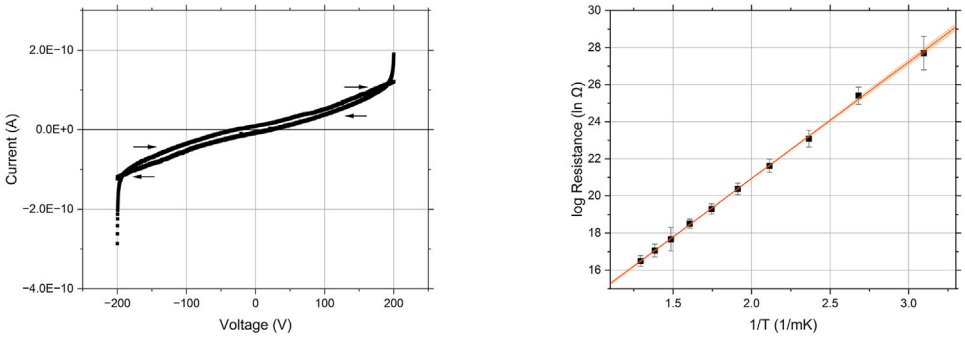

Figure 2. a) IV characteristics for the PRR-1M device type, displaying the high resistance (1.90 ± 0.01 TΩ) compared to the other NCN devices tested. b) The Arrhenius plot for the PRR-1M device type, with a calculated E_a of 540 ± 20 meV.

diamond's physical properties.[20,21] In contrast, femtosecond laser processing avoids heat dispersion, instead causing electrons to briefly ionize and cleave the C—C bonds. This allows a variety of allotropes, including graphite and amorphous carbon, to form upon relaxation.[18,19,22] This mechanism results in highly confined features within the diamond, enabling the fabrication of electrically active 3-D architectures within the bulk material without disrupting the surrounding crystal.

The specific carbon allotropes produced within the diamond, and thus the resulting NCN's electrical properties, are entirely dependent on the applied laser parameters. While power density is a primary factor, the precise relationship between laser input and material outcome is not always straightforward. For instance, Kuriakose et al. reported that longer pulse lengths generally produced more conductive tracks, suggesting that more graphite is formed at lower peak power densities, while also identifying a 'sweet spot' for pulse energy that resulted in minimal resistivity.[23] In femtosecond laser processing, the pulse repetition rate (PRR) also has a pronounced impact on the effective power density delivered to the focal volume. This study specifically investigates the profound impact of PRR on NCN electrical properties, probing the role of the previously identified diaphite' phase, with its reported ambipolar characteristics, in tuning the electrical response.[24,25]

Further detail on the formation of these NCN structures is given in the extensive review by Ashikkalieva et al., and these structures have already found use in diamond-based radiation detectors.[26–28] However, in many studies to date, diamond's high refractive index (n = 2.42) causes the laser spot to 'de-focus', restricting the use of laser-processing to surface restructuring or vertical, 1-D wires' running through the diamond.[29–31] Fully 3-D buried architectures can be achieved by using adaptive optics to compensate for spherical aberration induced at the diamond interface, allowing for more complex structures and expanding the applications of this technique.[32]

In this work, it is demonstrated that the properties of individual NCNs can be tuned by altering the laser parameters, notably the PRR. This allows for the formation of both conductive and apparently semiconductive material using a single fabrication process. Furthermore, laser processing conditions which create an NCN variant that displays ambipolar characteristics are reported. This behavior was briefly discussed in the authors' previous work exploring the NCNs' atomic structure, with the electrical characteristics and applications of this material more fully investigated here.[33] This opens the door for more complex, transistor-like architectures. Such a device is also presented, where the entire active portion of the transistor encapsulated within the diamond substrate. The success of this pilot device shows promise for the future development of a complete suite of robust, all-carbon electronics.

2. Results and Discussion

2.1. Results

The first NCN devices tested were isolated vertical columns through the substrate fabricated with a laser PRR of 1 kHz, termed PRR-1k, to allow comparison to the results reported in Sun et al.[32] These devices displayed good Ohmic conductivity, as shown in **Figure 1a**, with an average resistance of 76(± 8) kΩ. The diameter of the columns inside the diamond was measured optically to be 2 μm, giving a calculated resistivity of the material as 1.4×10^{-3} Ωm, two orders of magnitude higher than the resistivity of pure crystalline graphite, $3 - 60 \times 10^{-5}$ Ωm.[34]

However, an SEM study of similar laser-written material by Ashikkalieva et al. has shown that the true structure of the laser-written tracks is not a continuous graphitic cylinder, but in fact an overlapping series of graphitic sheets roughly 75 nm thick, formed along the fractured (111) diamond planes at 35.4° to the laser axis.[21] This internal structure is further supported by the findings of a TEM study of the PRR-1k material.[33] Using this model for the conductive channel, as shown in Figure 1c, the resistivity is calculated as 1.3×10^{-5} Ωm, in much better agreement to the value for crystalline graphite and providing confidence that this device (PRR-1k) is simply a continuous graphitic channel, albeit with a complex internal structure. Figure 1b shows the Arrhenius plot for the PRR-1k device type, obtained via impedance spectroscopy (IS) showing a very shallow gradient resulting in a thermal activation energy of 4.9(±0.2) meV, consistent with the graphitic, semi-metallic conduction observed.

Devices based on initial laser-written tracks using a 1 MHz laser pulse repetition rate at the same pulse energy, in this case the PRR-1M (a single pass track at a PRR of 1 MHz), gave incredibly high resistances (>1 TΩ); very different to those based on the

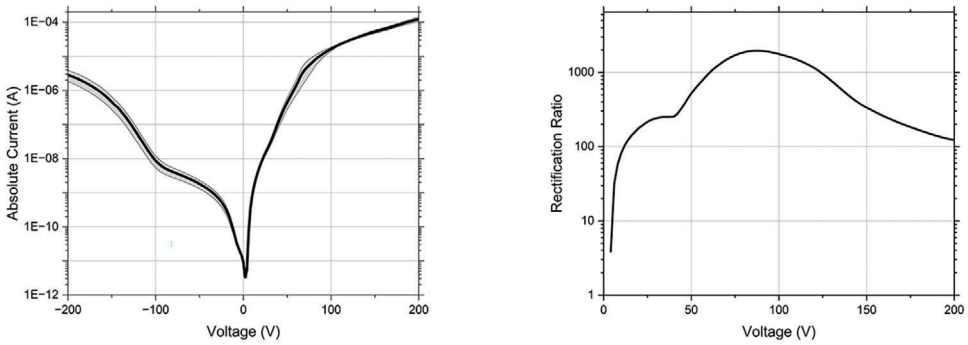

Figure 3. a) I–V characteristics for the PRR-1k1M devices, showing an asymmetric voltage response. The shaded portion represents the standard error across the seven devices tested. b) The rectification ratio of the PRR-1k1M diode against voltage, showing peak rectification around 90 V.

PRR-1k NCNs mentioned above. This result was initially unexpected, as the expectation was the 1000 × higher incident power, in terms of a photon-pulse arrival rate, would result in more sp^2 formation and hence an even more conductive track. As an example, **Figure** 2a shows the IV characteristics for the PRR-1M device type, giving the high resistance of 1.90 ± 0.01 TΩ. Nevertheless, Figure 2b shows that the PRR-1M material exhibits an entirely different IS behavior to the PRR-1k columns, with a measurable E_a of 0.54 ± 0.02 eV, hinting at a semiconductive nature. This value is not too dissimilar to that of conventionally doped semiconducting diamond.[11–13]

It has been shown previously that repeated exposures of the same diamond volume can continue to modify the material, generally resulting in an increased conductivity.[32] However, overwriting an existing NCN with a different set of laser conditions opens up a whole new parameter space, and could have potentially drastic effects on NCN behavior. Most intriguingly, the PRR-1k1M devices, which are fabricated by fully overwriting an existing PRR-1k NCN channel with a PRR of 1 MHz, exhibited an entirely different IV response. In this case the current–voltage response was clearly asymmetric, i.e., diode-like. This pseudo-rectification is reminiscent of ambipolar systems, and was not present in either of the single write conditions, showing that this overwrite has successfully produced an altogether different NCN composition. The average current–voltage characteristics of the seven devices, fabricated on two different substrates, are shown in **Figure 3**. The ratio of forward/reverse currents reached 2500(±500), and the best performing device showed a ratio of over 5500. The peak current measured through the devices was 0.4 mA, giving an ON resistance of 500 kΩ with no breakdown observed up to ±200 V. This resistance gives a resistivity of 9.2 × 10^{-3} Ωm or 8.6 × 10^{-5} Ωm using the same models for the conductive NCN pathway as the PRR-1k device, shown in Figure 1c. Reversing the overwrite order to give PRR-1M1k columns, with an initial 1 MHz channel followed by a 1 kHz exposure, produced no change from the PRR-1M channels, and also resulted in resistances of >1 TΩ.

In order to stress test this pseudo-diode, the bias applied to the laser-side contact was continuously swept from −200 to 200 V and back again over 120 times. **Figure 4** shows the evolution of the voltage response during the testing. The peak forward current shows an initial drop from 260 µA to 170 µA over the course of the first 40 sweeps, after which it remains stable. The peak reverse current drops similarly, falling from 5.4 µA to 1.0 µA before stabilizing. Interestingly, the reverse current between −100 and 0 V opposes this trend, increasing over the course of the sweeps before plateauing around 3.2 nA, while still remaining low enough to maintain a high rectification ratio exceeding three orders of magnitude.

The PRR-1k1M devices were then also studied using IS. The impedance magnitude response at 0 V DC bias, and the corresponding Arrhenius plot, are given in **Figure** 5a,b, respectively. Despite the completely different IV behavior, the calculated E_a for the diodes is surprisingly similar to the insulating PRR-1M columns at 0.58 ± 0.02 eV. Applying a DC bias on top of the AC probe signal during the IS measurements allowed for the investigation of the NCN's E_a in

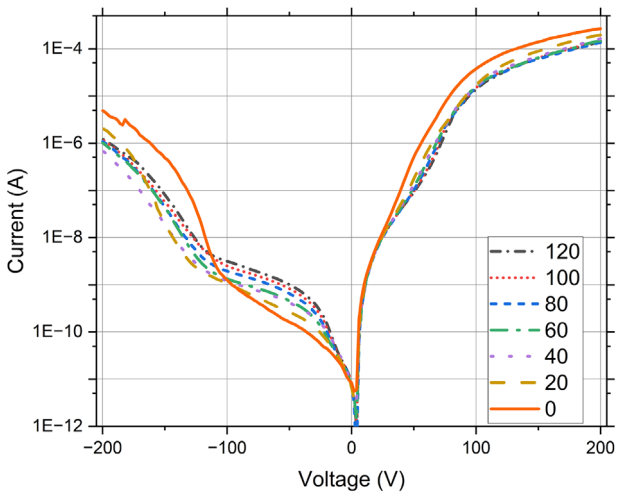

Figure 4. Stress test measurements on a PRR-1k1M diode over the course of 120 voltage sweeps. The legend provides the measurement number. The currents at ±200 V show minimal variation after the first 40 runs, while the reverse current between −100 V and 0 V increases over the course of the measurements, although still revealing greater than three orders of magnitude rectification ratio at a voltage of some 100 V.

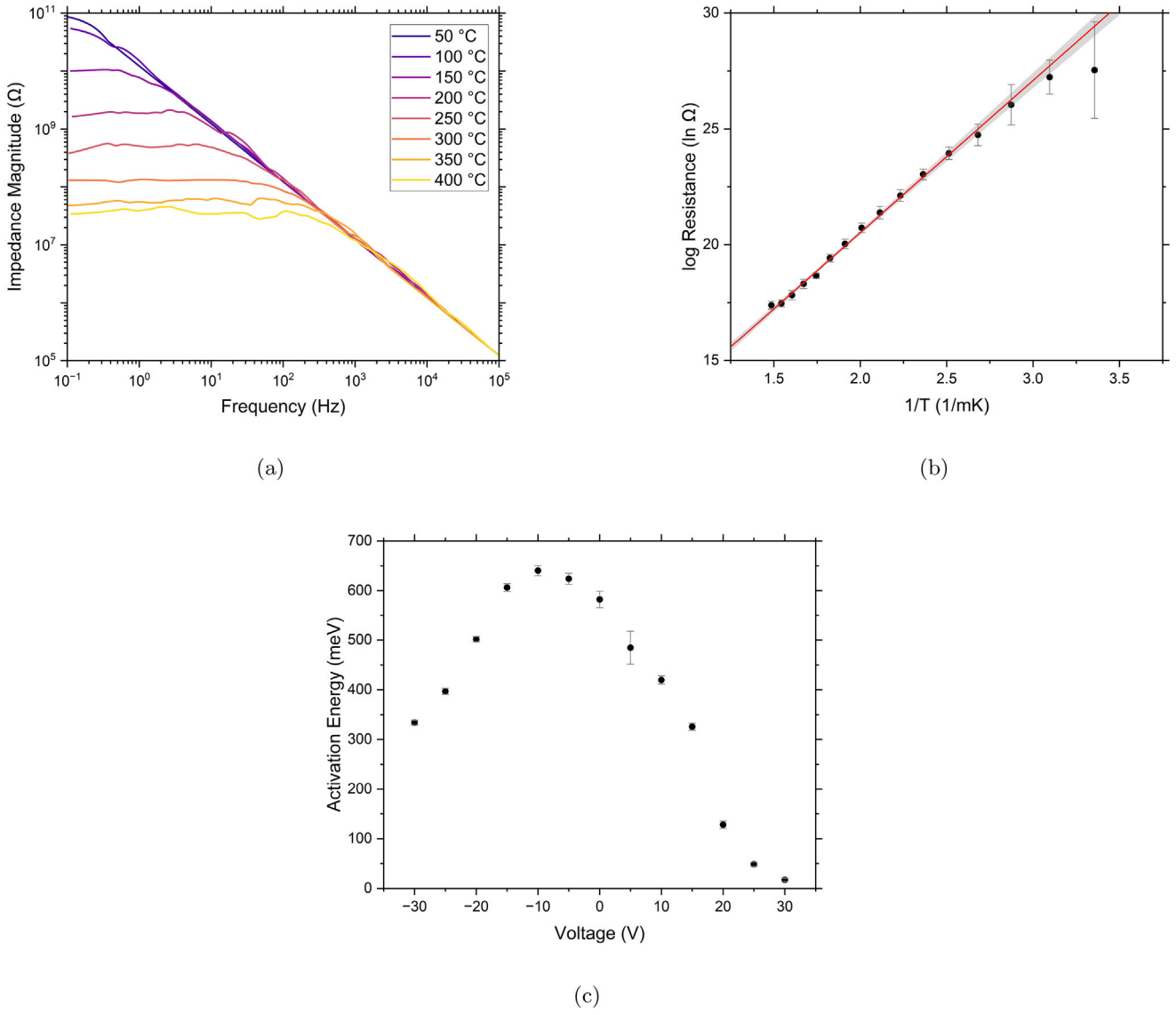

Figure 5. a) Bode plot of a PRR-1k1M device, showing decreasing impedance magnitude with increasing temperature. b) The PRR-1k1M Arrhenius plot for a single RC parallel circuit fit to the impedance spectroscopy data, with an applied linear fit in red. The 95% confidence interval is shown as the grey highlight. c) The calculated activation energy values for PRR-1k1M devices plotted against the DC bias applied during impedance spectroscopy measurements.

various different conductive regimes, with the corresponding data shown in Figure 5c. Interestingly, the peak activation energy value, and with it peak device resistance, was observed at −10 V, decreasing with both higher and lower applied biases. There is also a notable drop-off in activation energy when the bias changes from +15 to +20 V, with semi-metallic behavior displayed above +30 V ($E_a = 17 \pm 3$ meV).

To further explore the applications of this apparently ambipolar material, a field effect transistor (FET) architecture was devised and tested. A schematic of the device design is shown in **Figure 6**, made up of a cage-like gate structure written using the PRR-1k characteristics, separated by 5 µm of intrinsic diamond from a central column, which acts as the FET channel. This column was written similarly to the PRR-1k1M pseudo-diodes, but only the middle third of the PRR-1k structure was overwritten, with the hope that this would reduce the ON-resistance of the device. This proved successful, with a forward resistance of 7.9 MΩ. However, these structures underwent an irreversible breakdown at applied biases greater than roughly 25 V, with most devices subsequently becoming fully Ohmic and losing all semiconductor-like properties (Figure S1, Supporting Information). Nevertheless, the increase in conductivity of the central channel allowed for the testing of the functionality of the FET. **Figure 7a** shows the output characteristics of the FET for gate voltages between 20 and -20 V; whilst far from ideal transistor characteristics, clear modulation of the channel current is apparent. The maximum current density (J_{Max}) ranges from $J_{Max(V_G=20V)} = 23.8\ \mu A \mu m^{-2}$ to $J_{Max(V_G=-20V)} = 52.5\ \mu A \mu m^{-2}$.

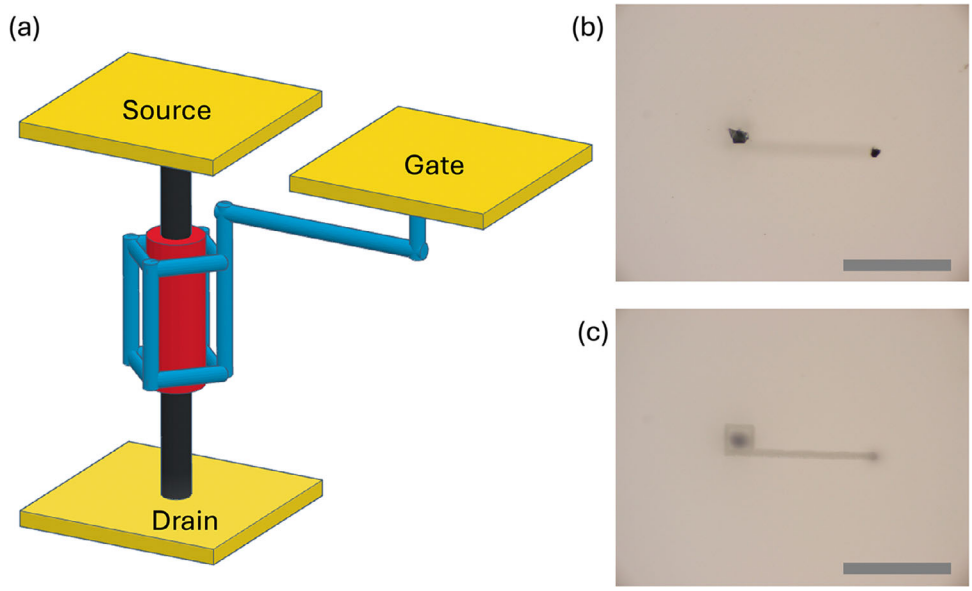

Figure 6. a) A schematic of the FET architecture. The central column comprises of a conductive track (black) laser written using air-based optics and a PRR of 1 kHz, followed by a partial overwrite (red) with the PRR set to 1 MHz to create a semiconducting channel roughly 100 µm long. The cage-like gate structure (blue) was then laser written using oil immersion optics and a PRR of 1 kHz, with a diamond layer no thinner than 5 µm between the two NCNs. The source, gate and drain contacts are labelled. Also shown are optical microscope images focused on the surface of the substrate (b) and the top of the internal gate structure (c). Both scale bars represent 50 µm.

The maximum measured transconductance (g_m) was 39.0(1) nS, found from the gradient of the plot shown in Figure 7b. While this value is low when compared to traditional silicon-based FETs, which typically exhibit values ranging from 10 to 500 mS, the authors emphasize the proof-of-concept nature of this device. There is also non-negligible leakage for both the $V_G = -20$ V and $V_G = +20$ V scans, but the gate current never exceeds 50% of the drain current even in the worst case (Figure 7c). Despite the relatively poor overall performance, the devices show the potential of this potentially paradigm-shifting approach to diamond electronics.

2.2. Discussion

These NCN-based devices represent fundamental steps toward an all-carbon suite of robust devices fabricated from diamond. This lower PRR material appears to have a higher sp^2 character than the other device types, resulting in its drastically increased conductivity when compared to the PRR-1M or PRR-1k1M devices. This is also supported by Raman spectroscopy, which was performed on the surface features of the three main NCN variants (PRR-1k, PRR-1M, and PRR-1k1M) in an attempt to explain the differences in their electronic behavior. The resulting spectra, as shown in Figure S2 (Supporting Information), indicate that the laser-written material remains largely sp^3 in character across all three devices, with slightly more sp^2 carbon formed in the PRR-1k writes than the others. This somewhat explains the considerably higher conductivity of the PRR-1k columns, but it must be noted that these measurements only provide information on the region where the NCN breaches the surface of the diamond substrate, and cannot inform information on the structure of the buried regions.

It should be noted, however, that the Raman data only provides information about the region where the NCNs breach the surface, and cannot give any indication as to the structure of the NCNs within the diamond bulk. The simple Ohmic conductivity of the PRR-1k NCNs will constitute one of the most basic and essential building blocks in future integrated carbon electronics. These structures are already providing measurable improvements in the performance of radiation detectors, combining the sensitivity of thin active regions with the stability and support of thick diamond substrates.[35,36] Metallic surface connections, which are so often points-of-failure in high-power devices, can be replaced by sub-surface graphitic channels, protected from the external environment and electrically insulated by the encapsulating diamond. Improvements to device breakdown voltage, a characteristic in which diamond electronics already excels, are also possible by allowing for increased distance between surface contacts while maintaining short active channels. Additionally, doped epilayers on diamond could be back-contacted, enabling true vertical device design and avoiding complex patterned etch technology or growth processes.[37,38]

The material produced by the PRR-1M conditions is altogether different, with its high resistivity and comparably large E_a. These measurements suggest that there is little-to-no continuous graphitic nature to these NCNs. Under these higher power conditions, it is likely that a partial conversion of any graphitic-like material back to the diamond phase may occur, along with substantial crystal damage through the introduction of threading dislocations. In such a case the lack of any continuous coherent sp^2 phase would explain the highly resistive nature of the "wires" despite the optical appearance of a continuous structure. The reformation of sp^3 carbon is further supported by the Raman spectra acquired for the three main NCN types studied, where the lower

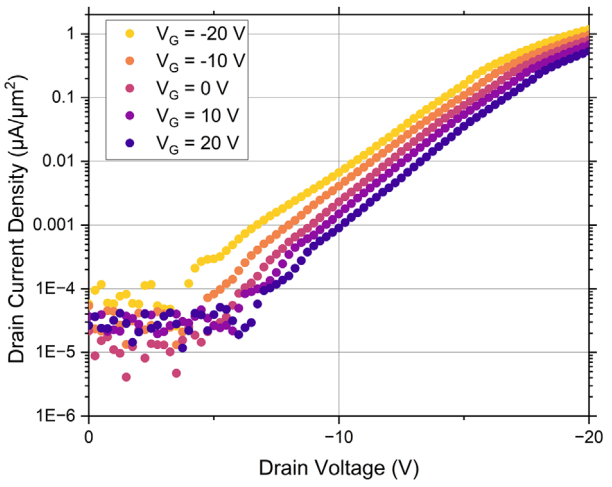

(a)

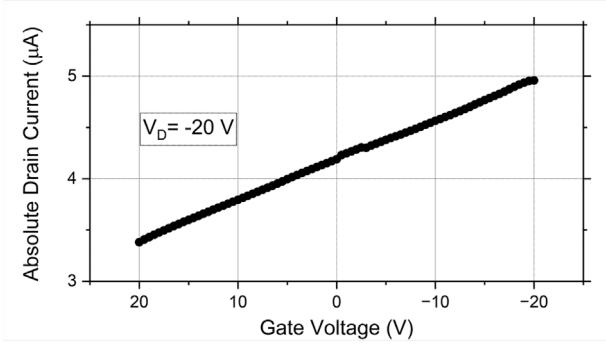

(b)

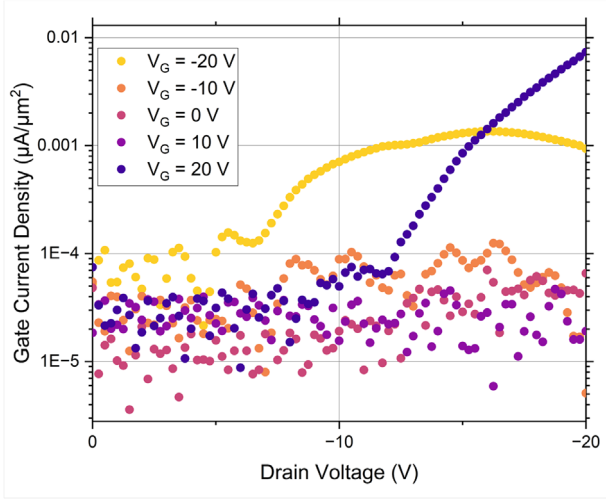

(c)

Figure 7. a) The forward operation of the FET for a range of applied gate voltages, showing clear modulation of the current density as the gate voltage is varied. The maximum current density, 1.17 μAμm⁻2, relates to a maximum current of 3.68 μA. b) shows the modulation of the drain current as the gate voltage is varied from 20 to -20 V, giving the maximum transconductance of the FET as 39.0(1) nS when the drain voltage is held at -20 V, and (c) shows the gate current density of the FET during operation, showing that, for most of the trialled gate voltages, the leakage current is never significant.

Table 1. The laser systems and processing parameters used for the NCN devices.

Laser System	Light Conversion Pharos SP-06-1000-pp	SpectraPhysics Solstice
Medium	Yb:KGW	Ti:Sapphire
Wavelength (nm)	515	790
Pulse Energy (nJ)	120	110
Pulse Width (fs)	170	250
Pulse Repetition Rate (Hz)	1×10^3 - 1×10^6	1×10^3
NA	0.5	1.4
Scan Speed (μm/s)	10	10
Use	PRR-1k, PRR-1M, PRR-1k1M columns	3-dimensional gate structure

FWHM for the PRR-1M and PRR-1k1M NCNs indicate a reduction in sp^2 material from that observed in the PRR-1k writes.

Despite this extreme resistivity, the existence of an available activation energy, as identified by IS, is potential evidence of a third phase wholly distinct from entirely sp^2 or sp^3 structures. Such a carbon allotrope has recently been identified, displaying the same electrical properties as identified here, and is something of an extended diamond-graphite interface with properties distinct from either bulk material.[25] This 'diaphite' phase, sometimes termed 'gradia', has been reported previously with a tuneable bandgap able to achieve the E_a measured in this work, provided the diaphite crystal structure is under considerable strain.[24] Considering this, alongside the findings of the authors' STEM/TEM investigation, the encapsulation of this diaphite phase within crystalline diamond would appear to provide sufficient strain to push the structure into its semiconductive regime.[33]

One of the exciting applications of this technology is presented in the PRR-1k1M devices, which exhibit diode-like asymmetric I–V characteristics. The overwrite with the higher PRR (1 MHz) introduces a non-continuous property to the sp^2 channel observed in the PRR-1k channels, in addition to the previously identified diaphite phase. With no applied DC bias, these NCNs show very similar properties to the PRR-1M channels being highly resistive. However, application of a bias overcomes the apparent barrier to conduction, with an activation energy as identified by IS. Thus, these all-carbon devices show that this apparent bandgap can be tuned by the application of an external DC bias, with a dependence on the polarity of such a bias. The behavior exhibited by this device type is again akin to an ambipolar semiconductor, where the material has more than one available charge carrier with different mobilities.[39] This is not entirely unexpected, with ambipolar behavior identified in other carbon systems such as graphene and carbon nanotubes (CNTs).[40,41] Femtosecond laser-processing may well produce CNT-like structures buried within the diamond, alongside the previously identified diaphite and graphenic domains. Unfortunately, all reported attempts to image NCNs have been limited to 2-D techniques such as SEM or TEM. Additionally, these imaging techniques have necessitated the use of milling techniques, which may alter or damage the NCN structure, such as FIB or mechanical grinding. For now, this leaves the exact 3-D structure of the NCNs up for debate, and imaging this

accurately will likely require the use of high-energy X-ray or neutron experiments.

A further characteristic of the PRR-1k1M pseudo-diodes, which must be emphasized is their consistency and reliability. In general, there was low variability across all laser-written devices of the same type, and the stress test performed on the PRR-1k1M channel shows that stability is not an issue with this technology, as it can be with other approaches to diamond electronics.[6,10] Testing was limited to ±200 V in this study due to available equipment, but future work will endeavor to identify the limits of irreversible breakdown for these devices.

The ability to successfully gate a central NCN channel using a separate buried structure is a major development of this technology. Ambipolar FETs have been produced previously, in the aforementioned graphene and CNT systems as well as more exotic interfaces such as that described by Wang et al.[42] Indeed, the behavior of these devices is closely mirrored by the laser-written, NCN-based device described here. While it is undeniable that the performance of this FET architecture leaves much to be desired, such as a true OFF-state and higher transconductance, this work stands as an exciting step into a new paradigm of all-carbon electronics. It is expected that the FET performance could be enhanced through design alterations such as reducing the gate-channel distance to increase transconductance, or minimizing the overwrite length to reduce ON-resistance. Through continued exploration of the laser parameter space, in addition to these design optimizations, a functional all-carbon FET device buried in diamond should be achievable.

It is interesting to note that the enhanced channel conduction with the application of negative gate voltages implies p-type characteristics dominate. Density functional theory modelling of the diaphite allotrope involves an electron transfer from the sp^3 carbon to the adjacent sp^2 phase, playing a role in the formation of the accessible bandgap exploited in the presented device's channel[25]. The p-type behavior observed implies that the transferred electrons do not play a major role in the conduction mechanism. As such, it is supposed that the basis for the semiconducting nature of the NCN channel is predominantly located on the diamond-side of the diaphite domains. This hypothesis requires further investigation with a wider range of structures and techniques before it can be fully understood, but this FET allows for an initial insight into the behavior of laser-written diaphite in a real-world setting.

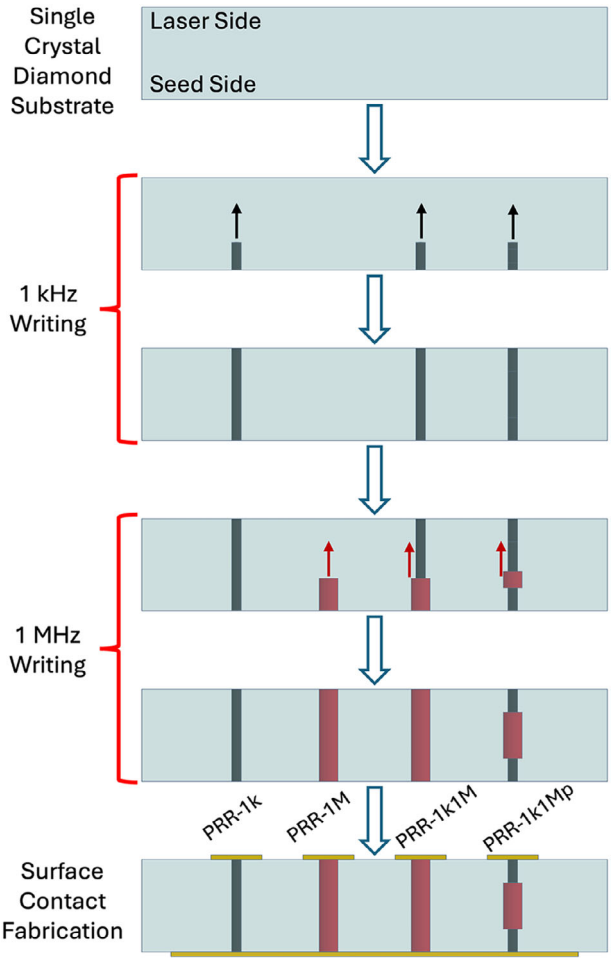

Figure 8. A fabrication process flow for the NCN column devices, showing the PRR-1k, PRR-1M, PRR-1k1M, and PRR-1k1Mp (the partial overwrite used for the FET channel). The first step was writing an array of PRR = 1 kHz columns into the single crystal diamond substrate, starting from the seed side (the lower surface) and drawing the laser spot up to the laser side (top surface). Next, the process was repeated with the PRR = 1 MHz setting, creating or overwriting the relevant columns to produce the studied devices. This was all performed using the Light Conversion Pharos SP-06-1000-pp laser, using the parameters outlined in Table 1. Finally, Ti/Pt/Au contacts were produced by electron-beam evaporation, using photolithographic methods to form discrete contacts on the laser side.

3. Conclusion

This research demonstrates the feasibility of using femto-second laser-processing to control the electrical properties of buried material inside diamond substrates, achieving both Ohmic and semiconductive/ambipolar behaviors. This technique provides a novel approach to creating electrically active diamond, circumventing the limitations of traditional doping. The successful fabrication of a buried, all-carbon transistor architecture within bulk diamond highlights the potential for developing electronic devices suitable for many harsh environment applications. This work represents a significant step towards realizing robust, all-carbon electronics. Future studies will focus on optimizing device performance and exploring applications in specific harsh environments such as high-temperature and high-radiation conditions.

4. Experimental Section

Substrate Acquisition: The substrates used in this work were 4 × 4 × 0.4 mm electronic grade CVD diamond plates ($B < 1$ ppb, $N < 10$ ppb, $R_a < 3$ nm, Chenguang Machinery Ltd).

Laser-Writing of Internal Structures: The laser-processing of these diamond substrates was performed using two adaptive optical setups, with the parameters laid out in **Table 1**. For any vertical channels which spanned the entire height of the substrates, an Yb:KGW laser (Light Conversion Pharos SP-06-1000-pp) was used with a central wavelength of 515 nm, a pulse duration of 170 fs, and a pulse energy of 120 nJ. The light was focused through a microscope objective (Zeiss 20×, 0.5 NA), resulting in a laser

spot approximately 0.6 µm across (x-, y-axis) and 9.8 µm deep (z-axis) inside the diamond. The laser's PRR was varied between 1 kHz and 1 MHz to fabricate the NCNs with different electrical behaviors. The diamond sample was mounted on 3D precision translation stages (Aerotech ABL10100 (*x*,*y*); ANT95-3-V (*z*)) and moved downwards at 10 μms^{-1}, 'drawing' the NCN from the back surface to the top. Over-writing of previously written NCNs was also performed, by re-tracing the original stage motion using a different PRR setting. This process is outlined in **Figure 8**.

The remaining structures, namely the 3D internal gate for the FET architecture, were written using a Ti:sapphire laser (SpectraPhysics Solstice) with a wavelength of 790 nm, pulse duration of 250 fs and 1 kHz repetition rate focused by a 1.4NA oil-immersion objective lens. This setup was used with a pulse energy of 110 nJ, and a laser spot size of approximately 0.3 µm across and 2 µm in the z-axis. This tighter axial confinement allows for accurate fabrication inside the diamond without requiring seeding of the diaphite structures from a surface. Hence this setup was favored during fabrication of the 3-D portions of the FET architecture. The stage speed remained at 10 μms^{-1}.

Substrate Cleaning and Contact Preparation: After the laser-processing, the substrates were cleaned in a boiling acid solution (H_2SO_4:$(NH_4)_2SO_4$ at 200 °C for 20 min) to remove any debris produced by the fabrication and to allow a clean contact to the surface NCN features.[43] Subsequently, the substrate underwent an ozone treatment (200 °C, 50 mbar, 1 h) to oxygen terminate the surface, preventing STD-based conduction and effectively isolating each device.

Discrete Ohmic contacts (Ti/Pt/Au, 20:5:200 nm thickness, Edwards A500 Electron Beam Evaporator) were prepared on the top surface of the substrate using a photolithographic lift-off process (Heidelberg DWL 66+). A common contact on the opposite surface was used to permit access to the backside of the NCN channels. To ensure low contact resistance and reliable Ohmic contact, the Ti/Pt/Au contacts were annealed at 600 °C in vacuum for 1 h.[44] Microscope images of the laser-written columns before and after metal contact fabrication are shown in Figure S3 (Supporting Information).

Data Acquisition and Analysis: Current–Voltage (*I*–*V*) measurements were recorded using a Tektronix Keithley 4200-A SCS and an Evergreen EB-6 probe station, supplied by Lambda Photometrics Ltd. Impedance spectroscopy (IS) measurements were taken using a Solartron 1260 Frequency Response Analyzer connected to a 1296A Dielectric Interface. Measurements were taken in a custom-built vacuum chamber operated at 10^{-7} mbar. Frequency sweeps from 10 MHz to 100 mHz were performed at a range of temperatures, as well as a range of applied DC biases. Charge carrier activation energies (E_a) for each device type studied were found using the Arrhenius equation, where E_a is calculated from the gradient of $ln(Z)$ versus $1/T$, where Z is the impedance magnitude found by an equivalent circuit fitting of the impedance spectroscopy data.

Supporting Information

Supporting Information is available from the Wiley Online Library or from the author.

Acknowledgements

The UKs Engineering and Physical Sciences Research Council (EPSRC) is acknowledged for the award of a PhD studentship to CSH (EP/R513143/1), supervised by RBJ. EPSRC was also acknowledged for the award of a research grants to RBJ (EP/X00029X/1), PSS (EP/W025256/1), and CSH (EP/W524335/1) which partially supported this work. This work had been carried out within the framework of the EUROfusion Consortium, funded by the European Union via the Euratom Research and Training Programme (Grant Agreement No 101052200 — EUROfusion). Views and opinions expressed were however those of the author(s) only and do not necessarily reflect those of the European Union or the European Commission. Neither the European Union nor the European Commission could be held responsible for them.

The authors thank Dr. Alex Pakpour-Tabrizi for fruitful discussions and preliminary work enabling this research. Lambda Photometrics Ltd and Everbeing International Corporation were gratefully acknowledged for the loan of an Everbeing EB-6 DC probe station. Finally, the LCN Cleanroom was acknowledged for the use of equipment and for the invaluable assistance of the technicians.

Conflict of Interest

The authors declare no conflict of interest.

Data Availability Statement

The data that support the findings of this study are available from the corresponding author upon reasonable request.

Keywords

ambipolar, diamond, diaphite, diodes, laser-processing, nanocarbon networks (NCNs), transistors

Received: April 14, 2025
Revised: July 26, 2025
Published online:

[1] B. Baliga, *IEEE Electron Device Lett.* **1989**, *10*, 455.
[2] J. Y. Tsao, S. Chowdhury, M. A. Hollis, D. Jena, N. M. Johnson, K. A. Jones, R. J. Kaplar, S. Rajan, C. G. Van de Walle, E. Bellotti, C. L. Chua, R. Collazo, M. E. Coltrin, J. A. Cooper, K. R. Evans, S. Graham, T. A. Grotjohn, E. R. Heller, M. Higashiwaki, M. S. Islam, P. W. Juodawlkis, M. A. Khan, A. D. Koehler, J. H. Leach, U. K. Mishra, R. J. Nemanich, R. C. N. Pilawa-Podgurski, J. B. Shealy, Z. Sitar, M. J. Tadjer, et al., *Adv. Electron. Mater.* **2018**, *4*, 1600501.
[3] P. W. May, *Philos. Trans. R. Soc. London, Ser. A* **2000**, *358*, 473.
[4] C. J. H. Wort, R. S. Balmer, *Mater. Today* **2008**, *11*, 22.
[5] W. De Boer, J. Bol, A. Furgeri, S. Müller, C. Sander, E. Berdermann, M. Pomorski, M. Huhtinen, in *Physica Status Solidi (A) Applications and Materials Science*, vol. *204*, Wiley-VCH Verlag GmbH, Germany, **2007** pp. 3004–3010.
[6] D. Araujo, M. Suzuki, F. Lloret, G. Alba, P. Villar, *Materials* **2021**, *14*, 7081.
[7] S.-W. Kim, R. Takaya, S. Hirano, M. Kasu, *Appl. Phys. Express* **2021**, *14*, 115501.
[8] L. Bäni, A. Alexopoulos, M. Artuso, F. Bachmair, M. Bartosik, J. Beacham, H. Beck, V. Bellini, V. Belyaev, B. Bentele, E. Berdermann, P. Bergonzo, A. Bes, J. M. Brom, M. Bruzzi, M. Cerv, G. Chiodini, D. Chren, V. Cindro, G. Claus, J. Collot, J. Cumalat, A. Dabrowski, R. D'Alessandro, D. Dauvergne, W. De Boer, C. Dorfer, M. Dünser, V. Eremin, R. Eusebi, et al., in *Journal of Instrumentation*, vol. *13*, Institute of Physics Publishing, IOP Publishing, Bristol, UK **2018**, pp. C01029–C01029.
[9] A. Traoré, P. Muret, A. Fiori, D. Eon, E. Gheeraert, J. Pernot, *Appl. Phys. Lett.* **2014**, *104*, 052105.
[10] N. Donato, N. Rouger, J. Pernot, G. Longobardi, F. Udrea, *J. Phys. D: Appl. Phys.* **2020**, *53*, 9.
[11] S. Bhattacharyya, O. Auciello, J. Birrell, J. A. Carlisle, L. A. Curtiss, A. N. Goyette, D. M. Gruen, A. R. Krauss, J. Schlueter, A. Sumant, P. Zapol, *Appl. Phys. Lett.* **2001**, *79*, 1441.
[12] Y. Katamune, D. Mori, D. Arikawa, A. Izumi, T. Shimaoka, K. Ichikawa, S. Koizumi, *Appl. Phys. A: Mater. Sci. Process.* **2020**, *126*, 11.

[13] T. H. Borst, O. Weis, *Phys. Status Solidi A* **1996**, *154*, 423.
[14] Y. T. Lee, A. Vardi, M. Tordjman, *Appl. Phys. Lett.* **2020**, *117*, 20.
[15] J. Zhang, J. Liu, Q. He, Z. Ren, K. Su, J. Zhang, Y. Hao, in *Sixth Symposium on Novel Optoelectronic Detection Technology and Applications*, vol. *11455*, SPIE, Bellingham **2020**, pp. 1745–1751.
[16] K. G. Crawford, D. Qi, J. McGlynn, T. G. Ivanov, P. B. Shah, J. Weil, A. Tallaire, A. Y. Ganin, D. A. Moran, *Sci. Rep.* **2018**, *8*, 1.
[17] R. J. Watkins, C. S. Henderson, A. C. Pakpour-Tabrizi, R. B. Jackman, *Appl. Phys. Lett.* **2023**, *122*, 093503.
[18] C. B. Schaffer, A. Brodeur, E. Mazur, *Meas. Sci. Technol.* **2001**, *12*, 1784.
[19] Y. Shimotsuma, M. Sakakura, S. Kanehira, J. Qiu, P. G. Kazansky, K. Miura, K. Fujita, K. Hirao, *J. Laser Micro/Nanoeng.* **2006**, *1*, 181.
[20] C.-Z. Wang, C. Z. Wang, C. Wang, C. Wang, K. M. Ho, K. M. Ho, K.-M. Ho, M. D. Shirk, M. D. Shirk, P. A. Molian, *Phys. Rev. Lett.* **2000**, *85*, 4092.
[21] K. Ashikkalieva, T. Kononenko, E. Ashkinazi, E. Obraztsova, A. Mikhutkin, A. Timofeev, V. Konov, *Diamond Relat. Mater.* **2022**, *128*, 109243.
[22] B. C. Stuart, M. D. Feit, S. Herman, A. M. Rubenchik, B. W. Shore, M. D. Perry, *Phys. Rev. B* **1996**, *53*, 1749.
[23] A. Kuriakose, A. Chiappini, B. Sotillo, A. Britel, P. Aprà, F. Picollo, O. Jedrkiewicz, *Diamond Relat. Mater.* **2023**, *136*, 110034.
[24] B. Yang, Y. Su, Z. Wang, L. Zhao, N. Hu, *Mater. Today Physics* **2022**, *28*, 100879.
[25] Z. Zhai, C. Zhang, B. Chen, Y. Xiong, Y. Liang, L. Liu, B. Yang, N. Yang, X. Jiang, N. Huang, *Adv. Funct. Mater.* **2024**, *34*, 2401949.
[26] K. K. Ashikkalieva, *Phys., Wave Phenom.* **2022**, *30*, 1.
[27] M. Girolami, L. Criante, F. Di Fonzo, S. Lo Turco, A. Mezzetti, A. Notargiacomo, M. Pea, A. Bellucci, P. Calvani, V. Valentini, D. M. Trucchi, *Carbon* **2017**, *111*, 48.
[28] R. J. Watkins, P. S. Salter, R. J. Moors, R. B. Jackman, *Sci. Rep.* **2025**, *15*, 8496.
[29] S. Kumar, B. Sotillo, A. Chiappini, R. Ramponi, P. Di Trapani, S. M. Eaton, O. Jedrkiewicz, *Appl. Phys. A: Mater. Sci. Process.* **2017**, *123*, 11.
[30] S. Kumar, S. M. Eaton, M. Bollani, B. Sotillo, A. Chiappini, M. Ferrari, R. Ramponi, P. Di Trapani, O. Jedrkiewicz, *Sci. Rep.* **2018**, *8*, 14021.
[31] O. Jedrkiewicz, S. Kumar, S. Kumar, B. Sotillo, M. Bollani, A. Chiappini, M. Ferrari, R. Ramponi, P. Di Trapani, S. M. Eaton, S. M. Eaton, *Opt. Mater. Express* **2017**, *7*, 1962.
[32] B. Sun, P. S. Salter, M. J. Booth, *Appl. Phys. Lett.* **2014**, *105*, 23.
[33] P. S. Salter, M. P. Villar, F. Lloret, D. F. Reyes, M. Krueger, C. S. Henderson, D. Araujo, R. B. Jackman, *ACS Nano* **2024**, *18*, acsnano.3c07116.
[34] D. C. Giancoli, *Physics: Principles with Applications*, 4th ed edn, Prentice Hall, Englewood Cliffs, N.J, **1995**.
[35] B. Caylar, M. Pomorski, P. Bergonzo, *Appl. Phys. Lett.* **2013**, *103*, 043504.
[36] C. Bloomer, M. E. Newton, G. Rehm, P. S. Salter, *J. Synchrotron Radiat.* **2020**, *27*, 599.
[37] M.-L. Hicks, A. C. Pakpour-Tabrizi, R. B. Jackman, *Sci. Rep.* **2019**, *9*, 15619.
[38] J. Canas, A. C. Pakpour-Tabrizi, T. Trajkovic, F. Udrea, D. Eon, E. Gheeraert, R. B. Jackman, *IEEE Trans. Electron Devices* **2021**, *68*, 6279.
[39] J. G. Champlain, *Appl. Phys. Lett.* **2011**, *99*, 123502.
[40] P. Avouris, *Chem. Phys.* **2002**, *281*, 429.
[41] J.-S. Moon, *Carbon Lett.* **2012**, *13*, 17.
[42] C. Wang, S. Yang, W. Xiong, C. Xia, H. Cai, B. Chen, X. Wang, X. Zhang, Z. Wei, S. Tongay, J. Li, Q. Liu, *Phys. Chem. Chem. Phys.* **2016**, *18*, 27750.
[43] B. Baral, S. S. M. Chan, R. B. Jackman, *J. Vac. Sci. Technol., A* **1996**, *14*, 2303.
[44] P. E. Viljoen, *J. Vac. Sci. Technol. B Microelectron. Nanometer Struct.* **1994**, *12*, 2997.